SUBDUCTION OF THE NAZCA PLATE BENEATH PERU
AS DETERMINED FROM SEISMIC OBSERVATIONS

Akira Hasegawa* and I. Selwyn Sacks

Carnegie Institution of Washington, Department of Terrestrial Magnetism
Washington, D. C. 20015

Abstract. A detailed reinvestigation of seismicity in the southern half of Peru using data from a local seismic network and a focal mechanism study using P wave first motions reveal that for the first 100 km of descent the slab (as defined by this seismicity) enters at a normal dip angle near 30° and that below this depth it is bent to a nearly horizontal angle. This horizontal slab extends eastward for about 300 km and then dips steeply below the thick continental lithosphere. ScSp observations are found to be consistent with the profile of the subducting plate as determined from the local seismicity. Beneath the region from southern Peru to northern Chile, the Nazca plate descends with an almost constant dip angle (∿30°) down to at least 300-km depth. Between the 30° dipping plate in southern Peru and the horizontal profile beneath central Peru, there is a contortion over a 100-km-wide continuous lateral section of the subducting plate. We infer that, at least in the upper 150 km depth range, the descending Nazca plate is contorted rather than torn.

1. Introduction

Western South America is the only major subduction zone where an oceanic slab descends under a continent. Studying the subduction of the Nazca plate beneath this region provides information about the differences and the similarities between the subduction process of the oceanic slab beneath a continent as opposed to an island arc.

While there is agreement on the geometry of the subduction process beneath southern Peru and northern Chile, two conflicting models have been proposed for the subduction beneath central and southern Peru and central Chile. The first model [e.g., Barazangi and Isacks, 1976, 1979; Isacks and Barazangi, 1977; Isacks and Molnar, 1971; Stauder, 1975; Sykes, 1972], based mainly on the teleseismically determined seismicity, postulates a shallow-dipping inclined seismic zone with a dip angle of about 10°. The second model [e.g., James, 1978; Okada, 1973; Sacks, 1977; Snoke et al., 1977, 1979] is based principally on the analysis of ScSp waves, resulting from ScS-to-P conversions at the upper boundary of a descending slab, and it postulates a normal subduction with plate dip of about 30°.

The accuracy of hypocenter locations of the International Seismological Centre (ISC) and the U.S. Geological Survey (USGS) in this region, especially in focal depth, is poor due to the sparse distribution of nearby seismic stations, and this fact makes it difficult to interpret the subduction process beneath central Peru and cen-

tral Chile. Barazangi and Isacks [1976] proposed, by selecting the earthquakes located by the ISC and USGS with certain criteria, that well-located earthquakes define a shallow-dipping inclined seismic zone which extends inland from the trench. James [1978] questioned their event selection criteria and pointed out that a detailed study of the spatial distribution of earthquakes located by the USGS beneath central Peru shows that the seismicity beneath the continent tends to be confined to small, active clusters, one of those clusters forming a primary basis for the shallow subduction model.

On the other hand, Snoke et al. [1977] concluded from the analysis of ScSp waves that the Nazca plate has an approximately constant dip angle of about 30° in the region from central Peru to central Chile. Recently, Barazangi and Isacks [1979] suggested that no clear, consistent ScSp phases are observed at NNA in central Peru, the normal subduction model of Snoke et al. [1977] being based on the ScSp observations at this station. Snoke et al. [1979] made a detailed reexamination of ScSp data at this station and found that ScSp arrivals can be identified on all seismograms on which the predicted S/N ratio is greater than 1.

James [1978] pointed out in his normal subduction model beneath central Peru that the descending Nazca plate is nearly aseismic below about 90 km and that only small earthquakes would be expected to occur along the lithosphere-lithosphere boundary due to the direct contact of the two lithospheric plates. If this is the case, seismicity obtained by excluding small events like the Barazangi and Isacks [1976, 1979] one may not really delineate the deep seismic zone beneath Peru. Local seismic network data are essential to resolve this kind of controversy.

2. Spatial Distribution of Earthquakes Beneath Arequipa Network

a. Arequipa Seismic Network and Hypocenter Distribution Beneath It

A local net of nine stations was operated in 1965 by San Agustin University's Characato Observatory. The locations of the observation stations are shown in Figure 1. The data from this net are important because the area they cover includes portions of both categories of subduction zones, namely, southern Peru for which no disagreement exists and central Peru for which opposing models have been proposed.

Figure 2 shows the vertical section of the earthquakes located by more than five stations of the Arequipa net for the period from January to December 1965. The method used to locate these events is discussed in detail by James et al. [1969]. In both regions in Figure 2 the trend of

---

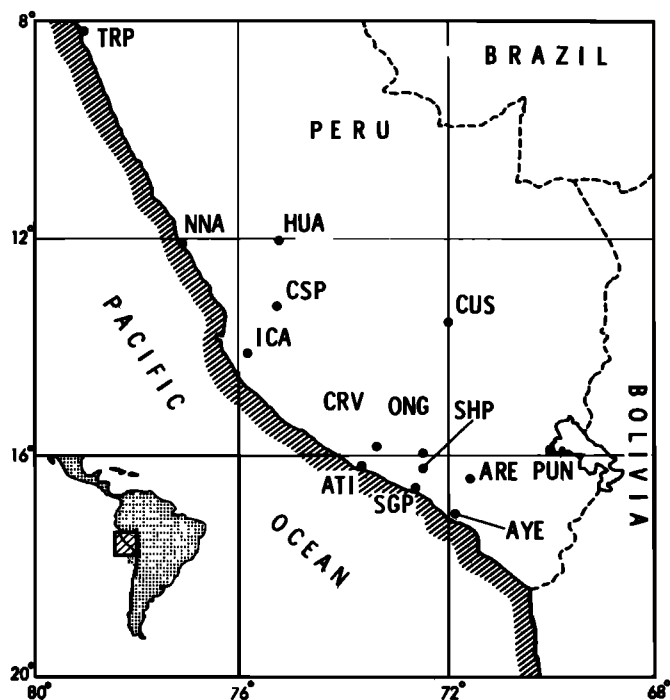*On leave from Tohoku University, Sendai, Japan.

Fig. 1. Location map showing seismic stations. The stations in the Arequipa net used in this study are CUS, CRV, ATI, ONG, SHP, SGP, PUN, ARE, and AYE.

standard earthquakes in order to estimate the source-region station correction at each station. The number of events thus adopted as standards was 61. The source-region station corrections for both P and S waves were then computed by averaging arrival time residuals of the standard events located in a rectangular region with a dimension of 50 x 100 km. Overlapping regions were averaged to obtain a station correction for each source region. All events with focal depths greater than 50 km were relocated using these source-region station corrections.

Figure 3 shows the vertical section of the earthquakes thus relocated. We can see from this figure that the deep seismic zone beneath the northern region (Figure 3a) dips with a normal dip angle near 30° above about 100-km depth and that, at this depth, it deforms and changes its dip angle to be approximately horizontal. The seismic activity along this deep seismic zone is continuous, and all the deep events which were located on the extension of the seismic zone above 100 km with a dip angle near 30° (Figure 2a) are relocated on this thinner seismic zone. It is reasonable to conclude therefore that all these earthquakes lie on the deep seismic zone and not in the continental lithosphere.

Beneath the southern region (Figure 3b), the scattered events eastward of the seismic plane in Figure 2b are relocated on the thinner seismic zone, and these events form its deeper portion. This deep seismic zone dips with a normal dip

deep seismic zone above 100 km extends into the deeper part with a constant dip angle of about 30°. There is other seismic activity above this seismic zone, as pointed out by James [1978]. Also, it may be seen in the northern region (Figure 2a) that the deep seismic zone bends and the dip angle decreases at a depth of about 100 km, which is similar to the seismicity selected by Barazangi and Isacks [1979]. Due to the scatter of the hypocenters, however, it is difficult to conclude which model this seismicity located by the local seismic network supports.

b. Relocation of Earthquakes Beneath the Arequipa Network

We attempted to eliminate the scatter in the hypocenter locations due to an inhomogeneous data set. This is particularly important in a region which may have structural heterogeneity or unknown structure. If this is not reflected in the velocity model used, the solutions will be biased by the particular ray paths used. Station corrections grouped by source region have been calculated in order that earthquake hypocenters can be accurately located relative to each other. The J-B velocity model was used. Other models (Herrin [1968] P table and Randall's [1971] S table) gave the same trend of hypocenters. The relocation procedure is as follows: First, we selected the events which are observed on at least seven of the nine Arequipa net stations. (Too few events were observed on eight or more stations to estimate adequately the source-region station corrections.) These earthquakes were carefully relocated by using the usual four-parameter method (S and P) and adopted as the
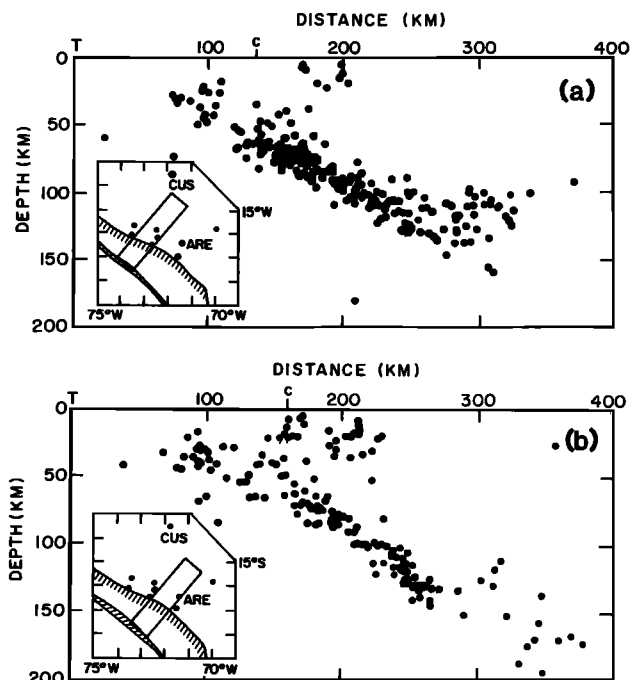

Fig. 2. Vertical cross sections of earthquakes located inside the rectangles on the inserted maps by more than five stations of the Arequipa network in southern Peru. Locations of seismic stations of the Arequipa network are shown by solid circles in the inserted maps. T and C denote trench axis and coast, respectively. The northern region (Figure 2a) and southern region (Figure 2b) correspond to the abnormal subduction and normal subduction areas, respectively.

angle of about 30° to a 200-km depth. From the present result and the seismicity of Barazangi and Isacks [1979] we conclude that the descending Nazca plate beneath central Peru dips at about 30° above 100-km depth then bends until it is nearly horizontal. In southern Peru-northern Chile, however, the Nazca plate descends with an almost constant dip angle of about 30° down to at least 300-km depth. The spatial distribution of the earthquakes determined using the local network observations is similar to that from selected teleseismic data [Barazangi and Isacks, 1979].

c. Contortion of the Descending Nazca Plate Beneath Southern Peru

We note that the apparent thickness of the deep seismic zone in Figure 3 increases in the inland region. This is mainly due to the contortion of the deep seismic zone in that region and the wide section shown. To investigate this, the northern and southern regions (Figures 3a and 3b) were each divided into four subregions. The earthquakes located in each subregion are plotted as vertical sections in Figure 4. The dip angle increases slightly from north to south and the deep seismic zone is now well confined. The solid curves in Figure 4 show the shape of the deep seismic zone inferred from the seismicity in each vertical section. For easier comparison, these subregions are superposed in Figure 5. The change in the shape of the deep seismic zone from north to south is easily seen. The change is greatest between region 3 and 6, but is everywhere continuous.

It is instructive to view the seismicity changes along strike as well. Figure 6 shows the seismicity in sections parallel to the

Fig. 4. Divided vertical cross sections of relocated earthquakes located inside the rectangles from regions 1 to region 8 on the inserted map. Solid curves show the shape of the seismic zone (below 50-km depth) inferred from the seismicity in each vertical section.
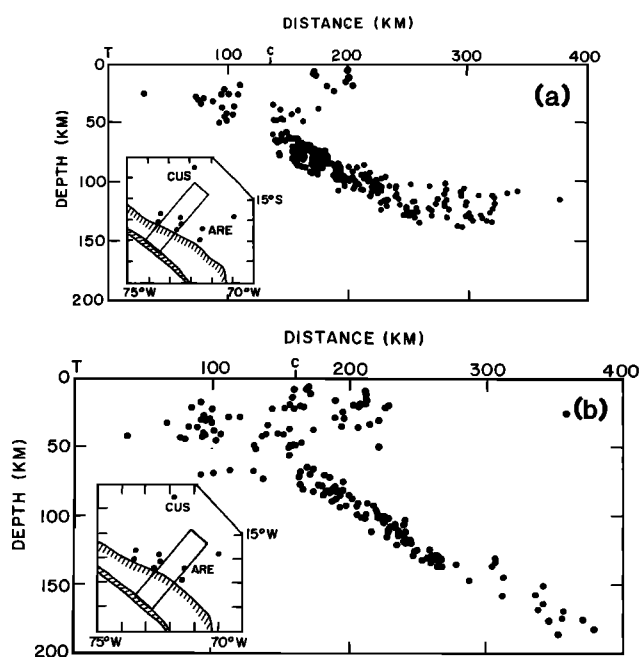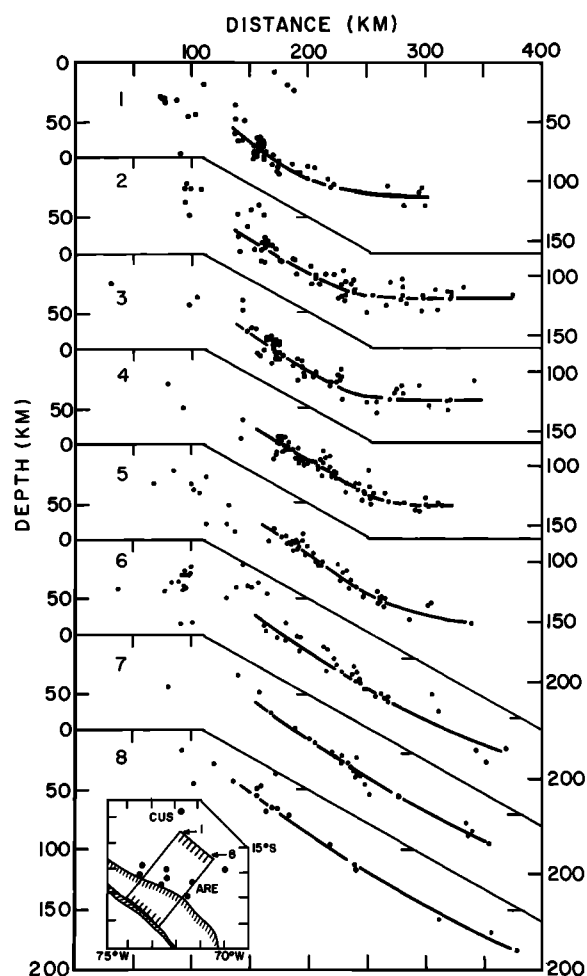

Fig. 3. Vertical cross sections of earthquakes relocated by using source-region station correction; otherwise as in Figure 2. Note that the spread in hypocenters is decreased.
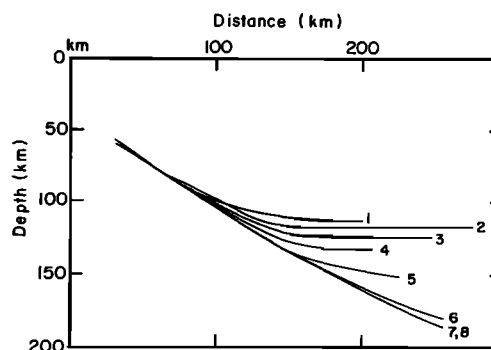

Fig. 5. Inferred shape of the deep seismic zone in each vertical section from region 1 to region 8 on the inserted map in Figure 4 showing how shape varies between the northern region and southern regions. The seismic plane, though deformed, is continuous.
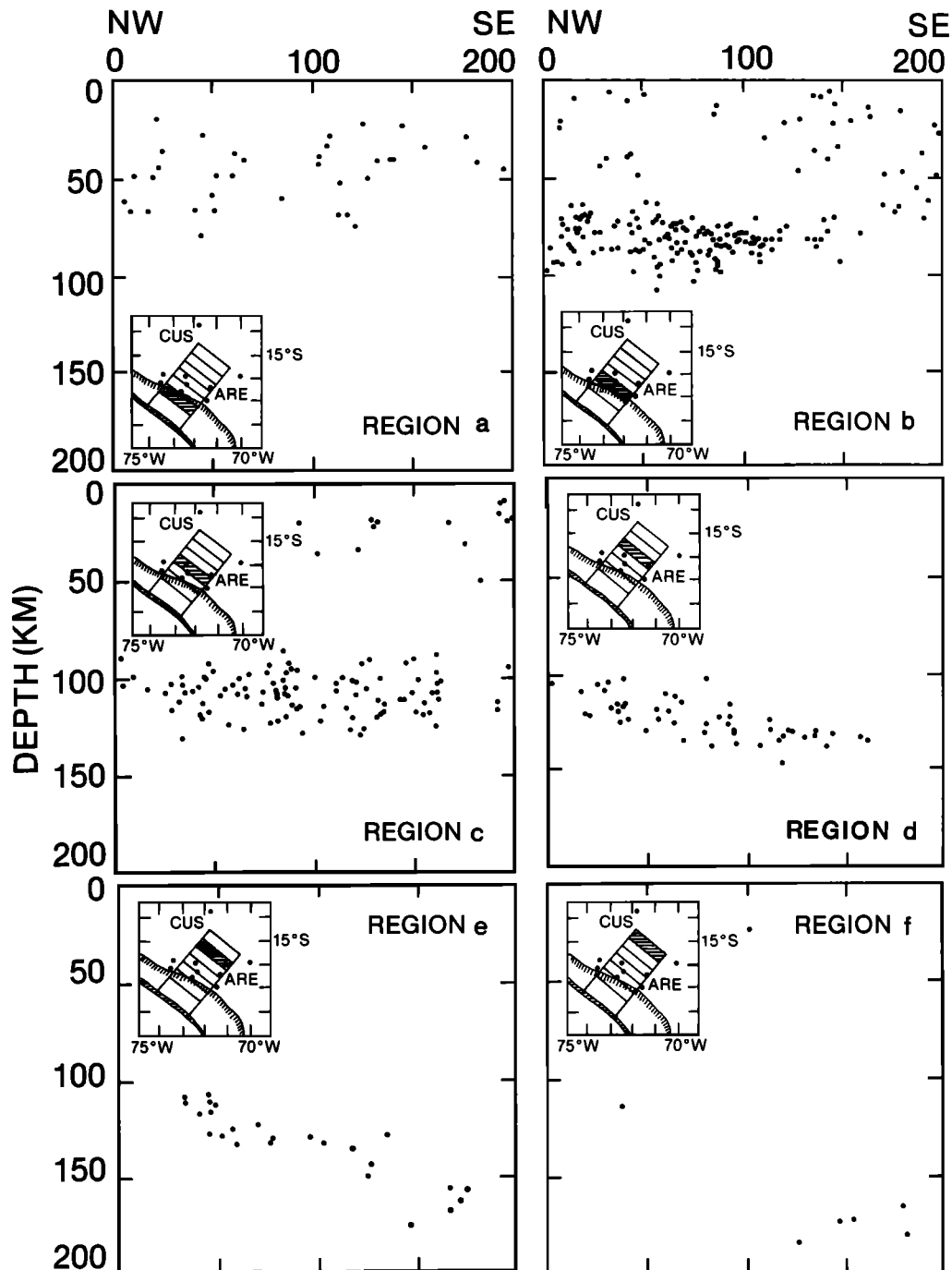
Fig. 6. Seismicity sections along the strike of the arc. The same data as in Figure 4 are shown. The hatched region is a plan of the seismicity shown. In Figures 6b and 6c the seismic band is essentially horizontal indicating planar (constant dip) subduction. In Figures 6d and 6e there is a pronounced inclination. This and the continuity of the seismicity in Figures 6d and 6e suggest a contortion.

trench. In this projection, continuous, planar seismicity will appear as horizontal bands of earthquakes; a tear will appear as a bimodal (discontinuous) distribution; a contortion will appear as a sloping band. At depths less than about 120 km (Figure 6b and 6c) the seismicity distribution is essentially a horizontal band. This indicates that the dip is constant over the whole section down to this depth. (This dip is

determined to be about 30° from Figure 3.) At greater depths (Figures 6d and 6e) the seismicity band shows a distinct slope, indicating a contortion, and remains continuous. There are too few earthquakes in Figure 6f to draw any further conclusions. It should be noted that about 400 earthquakes are shown in Figures 4 and 6 and that at least this many are needed to differentiate between a contortion and a tear. The con-

tortion of the Nazca plate is schematically shown in Figure 7. It is considered to be due to the transition from the nearly horizontal Nazca plate at the deeper part in the northern region to the more steeply dipping Nazca plate in the southern region.

Barazangi and Isacks [1979] suggested that there was a tear in the descending Nazca plate between region 4 and region 5 in Figure 4. However, our interpretation of the data is that it does not show a tear but rather delineates a contortion in a continuous slab. Such a precise structure can be detected only from local network data. The disruption of the Nazca plate into two segments may occur, if at all, below the depth range presented here.

3. Focal Mechanism Solutions

In order to understand the subduction process beneath an island arc or continent it is essential to investigate focal mechanisms of earthquakes occurring in the subduction region. Stauder [1975] determined focal mechanisms of earthquakes beneath Peru from P wave first motions and S wave polarization angles. Since there are not many earthquakes for which P and S wave data are available at widely distributed stations, the few solutions determined by Stauder do not allow complete understanding of the subduction process beneath Peru. An analysis of composite mechanism solutions of groups of small earthquakes for which individual mechanism solutions cannot be determined is therefore of great importance [e.g., Ritsema, 1955; Aki, 1966]. We next investigate the earthquake-generating stress field beneath Peru and its relation to the shape of the descending slab in detail by obtaining composite mechanism solutions for earthquakes in this region. About 300 well-located earthquakes selected by Barazangi and Isacks [1979] are analyzed. The number of P wave polarity data for these events is about 8000. The observations are from the ISC bulletins and are therefore mainly
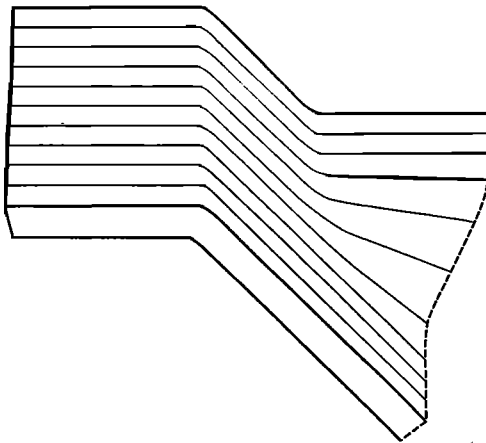
Fig. 7. Schematic model of the descending Nazca plate near the boundary between the nearly horizontal subduction zone beneath central Peru and the more steeply dipping subduction zone beneath southern Peru. In both regions the initial subduction angle is 30° and persists to at least 100 km.
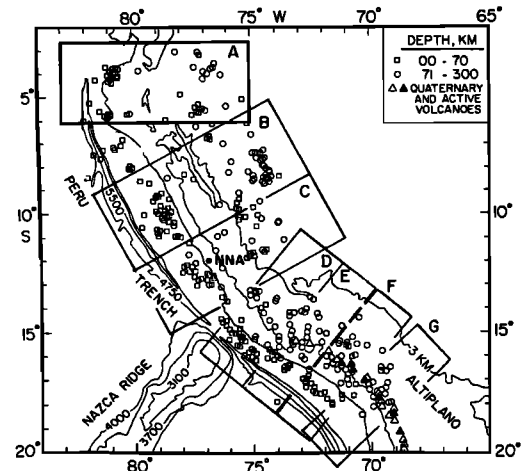
Fig. 8. Seismicity map in Peru showing events selected by Barazangi and Isacks [1979]. Locations of station NNA and seismic cross sections from A to G used for the composite mechanism study are shown.

teleseismic. The selection criteria and magnitude range of these events are described by Barazangi and Isacks [1979].

The seismic region is divided into seven subregions from A to G as shown in Figure 8, and the events located in each subregion are projected onto vertical sections approximately perpendicular to the local strike of the Peru trench. Earthquakes which are close to one another on the vertical sections and whose mechanism types are therefore presumed to be similar to each other are taken as a group, and P wave first motions of the earthquakes in the same group are superimposed on the same focal sphere. The earthquakes for which individual mechanism solutions were already determined by Stauder [1975] are excluded.

It is appropriate to discuss the assumptions implicit in the composite mechanisms method and their effect on the solutions obtained. In order to have sufficient data for a well-constrained solution, a number of earthquakes have to be considered as a single group. In the case of the somewhat sparse seismicity of the region considered, clusters (shown in Figure 9) may be 50 or
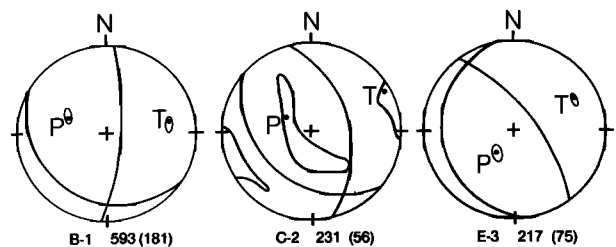
B-1 593(181)   C-2 231 (56)   E-3 217 (75)

Fig. 9. Composite focal mechanisms solutions for earthquake groups B-1, C-2, and E-3. The middle number is the number of data used; inconsistent data are shown in parentheses. The contours delineate the range of the P and T axes satisfying the data when any three data are reversed. C-2 and E-3 have similar numbers of data and inconsistent readings, but E-3 is a more stable solution. C-2 does suggest a horizontal tension axis, however.

even 100 km in extent. It is possible that there will be some variation in the focal mechanisms among these events which will lead to discordant data. This is particularly true in the vicinity of the nodal planes which tend to be zones rather than planes. In addition, for maximum coverage, much short-period data, which are of lower reliability, must be used.

The quality of the solution cannot be simply

related to the proportion of discordant data. We determine the stabilities of the solutions by testing their sensitivity to particular observations. Figure 9 shows the range of the P and T axes for some groups if any three observations are reversed. Solutions B-1 and E-3 are basically stable. C-2, which has similar data consistency to E-3, is less well-constrained but indicates that the T axis is probably near horizon-
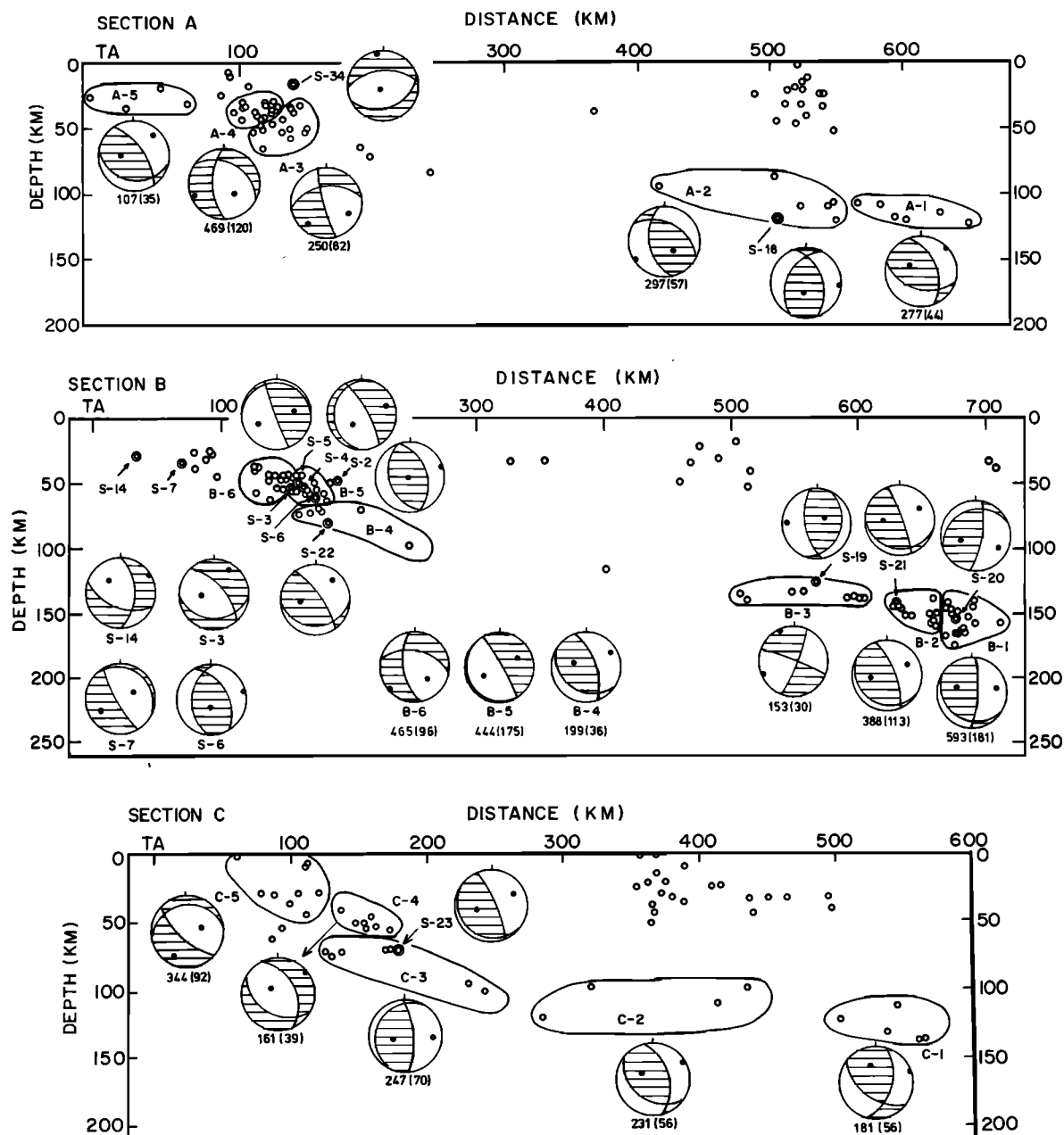

Fig. 10. Composite mechanism solutions on vertical cross sections for regions A to G shown on the map in Figure 8. Circles denote the hypocenter locations. Mechanism solutions for earthquake groups enclosed by solid curves are shown on the lower focal hemisphere by equal area projection. Shaded areas indicate quadrants of rarefaction first motion. The numeral in each solution denotes the number of P readings, and the numeral in parenthesis indicates the number of inconsistent stations for each mechanism solution. Mechanism solutions determined by Stauder [1975] are also included, the locations being shown by double circles.
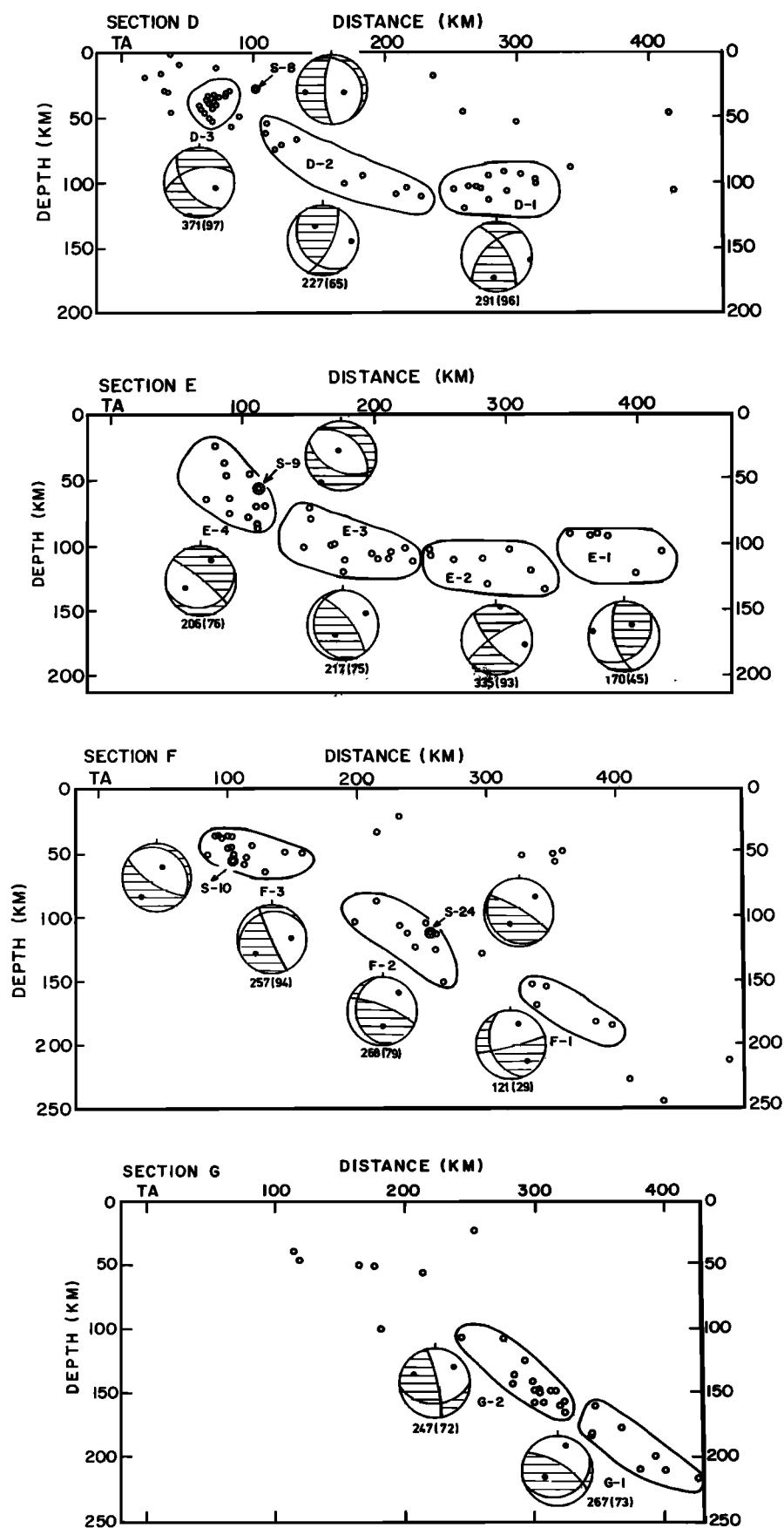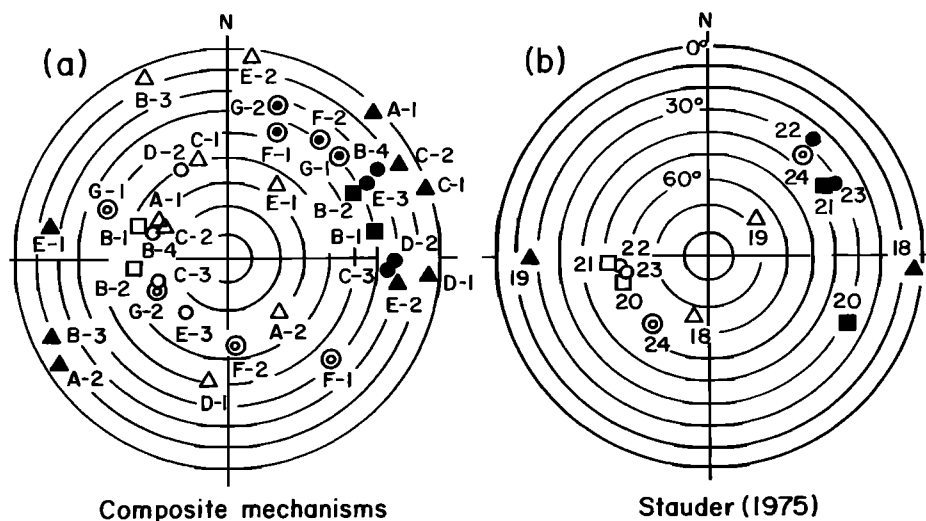
Fig. 10. (continued)

Fig. 11. Equal area projection of compression and tension axes for composite mechanism solutions (Figure 11a) and those determined by Stauder [1975] (Figure 11b) of intermediate depth earthquakes. The compression axis is represented by an open circle, triangle, square, and double circle, and the tension axis by solid symbols.

tal. Less stable solutions are rejected. In every case, the composite solutions agree well with Stauder's determinations.

The composite focal mechanisms obtained are shown on the vertical sections of earthquake hypocenters in Figure 10. Stauder's mechanism solutions for large earthquakes are also presented in the figure. The focal mechanism for group A-5 (under the Peru trench) indicates horizontal tension normal to the tectonic trend, which is considered to be caused by the flexure of the Nazca plate as it begins to bend. The shallow focus coastal earthquakes are characterized by reverse faulting, most of which are considered to represent underthrust of the continent by the Nazca plate on a shallow dipping thrust plane. Some of them (e.g., B-5 and E-4), however, indicate downdip compression. Isacks and Barazangi [1977] found this type of focal mechanism for the aftershocks of the May 31, 1970, Peru earthquake (in vertical section B) and interpreted it to be the result of elastic unbending of the descending Nazca plate. If this is the case, however, it is difficult to explain normal faulting mechanisms of earthquakes 2 and 6 in Stauder's paper (S-2 and S-6 in vertical section B), which are located in nearly the same location as the downdip compression type earthquakes.

The composite mechanism solutions for intermediate depth earthquakes indicate normal faulting or strike slip faulting, the trend of tension axis varying from the northeast to the east. The transition from shallow focus reverse faulting to this mechanism type occurs at about 70-km depth. Stauder [1975] classified focal mechanisms of intermediate depth earthquakes beneath Peru into two types: shallower foci of intermediate depth earthquakes have horizontal E-W tension axes; and the deeper foci are characterized by normal faulting with tension axis dipping about 30° and trending to the ENE, although there are several exceptions to this classification.

The present composite mechanism study reveals that the change in dip angle of tension axis for

intermediate depth earthquakes is closely related to the shape of the Nazca plate. Figure 11 shows the projection of tension and compression axes of intermediate depth earthquakes on the lower focal hemisphere. Earthquake groups in the subduction area with a plate dip of about 30° (vertical sections F and G in Figure 10) have tension axes dipping about 30° (double circle). Beneath the shallow subduction area (vertical sections A to E in Figure 10), earthquake groups in the coastal region, where the descending Nazca plate dips near 30°, also have tension axes dipping near 30° (circle), and those in the inland region, where the Nazca plate is almost horizontal, tend to have near horizontal tension axes (triangles). For easier comparison the dip angle of tension axis is plotted against the distance from the trench axis in Figure 12 for intermediate depth earthquakes in the shallow subduction area. The change in dip angle of tension axis from the coastal region to the inland region is clearly seen. It appears that the tension axis is nearly parallel to the local dip of the descending Nazca
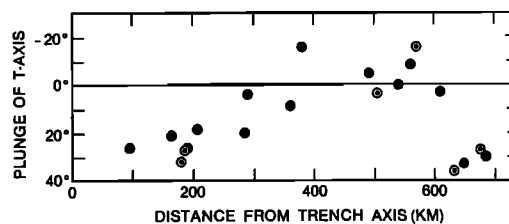

Fig. 12. Dip angle of tension axis (A-E) versus the distance from the trench axis for the intermediate depth earthquakes occurring in central Peru. Up to nearly 300 km east of the trench, the tension axis dips at 25°-30°. This corresponds to earthquake depths down to 100 km. Between 300 and 600 km east of the trench, the angle is essentially horizontal though there is considerable scatter in this range. Beyond 600 km, the axis dips 30°. Double circles are Stauder's solutions.
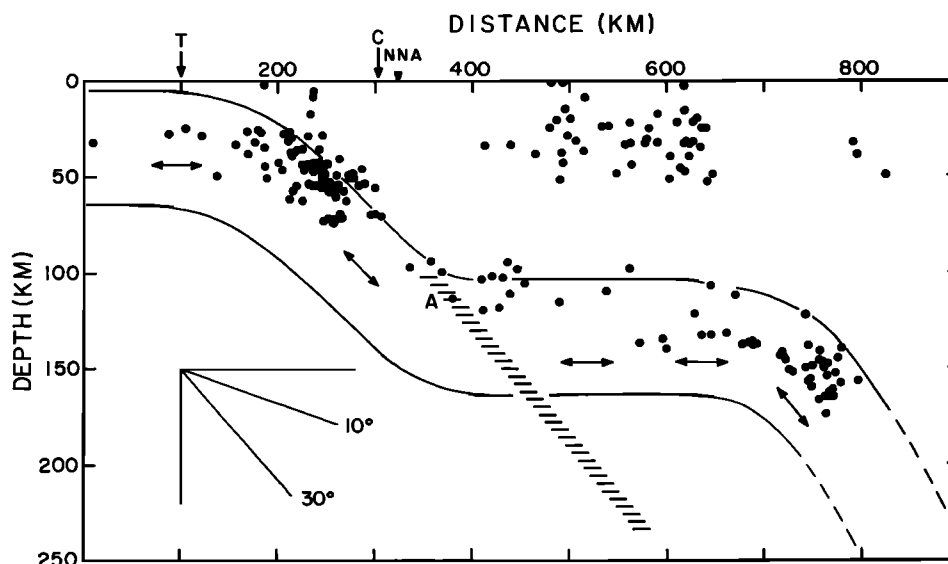
DISTANCE (KM)

Fig. 13. Cross section showing the inferred geometry of the descending Nazca plate beneath central Peru. Seismicity is from Barazangi and Isacks [1979]. This is a 1000 km wide section and therefore assumes the deformation in the slab constant over this width. The hatched zone denotes the possible conversion plane of the ScSp arrivals at station NNA (triangle) estimated by Snoke et al [1977]. Tension axes, shown by arrows, for focal mechanisms of intermediate depth earthquakes are approximately parallel to the local dip of the descending Nazca plate.

plate, although the compression axis scatters more widely. This is also the case for large earthquakes whose individual mechanism solutions were determined by Stauder (Figures 11b and 12).

Earthquake groups B-1 and B-2 (shown by squares) have tension axes dipping about 30°. These groups are located in the easternmost part of the region, and there the nearly horizontal Nazca plate seems to bend downward again (Figure 8b). Therefore earthquake groups B-1 and B-2 (and earthquakes 20 and 21 in Stauder's report) are also considered to indicate downdip extension. These mechanism solutions and the downward bending pattern of the easternmost part of the deep seismic zone may suggest the existence of an aseismic portion of the descending slab which extends to greater depth with a relatively steep dip angle, as illustrated in Figure 13 by broken lines. The descending Nazca plate seems to behave as a stress guide even in the shallow subduction region. The inferred earthquake generating stress field beneath central Peru is schematically illustrated in Figure 13 by thick arrows.

4. Comparison with Previous Models

In order to know whether our revised subduction model also explains the ScSp observations at NNA we reexamined the geometrical relationship between the location of the possible conversion plane for ScSp arrivals and that of the deep seismic zone beneath NNA. Figure 13 shows a vertical section of earthquakes selected in region 2 in central Peru by Barazangi and Isacks [1979]. Our model (solid curve) provides a good fit to this seismicity pattern. The possible conversion plane of ScSp arrivals at NNA [Snoke et al., 1977] is projected on this vertical section as a hatched zone. We have already men-

tioned in the previous section that the deep seismic zone in the northern region beneath the Arequipa network dips with a normal dip angle near 30° above about 100-km depth and that, at this depth, it bends rather abruptly and changes its dip angle to nearly horizontal (Figure 3). The configuration of the deep seismic zone beneath central Peru inferred from relatively large earthquakes (Figure 13) is quite similar to that located by the Arequipa network. Barazangi and Isacks [1979] interpreted the seismicity with the simplest possible model, regarding the descending Nazca plate as a gently dipping zone with an almost constant dip angle which extends inland for a distance of about 700 km from the trench. On the contrary, we consider that this relatively abrupt upward bending of the seismicity faithfully delineates the shape of the descending Nazca plate.

The upper boundary of the descending Nazca plate inferred from the seismicity shown by the solid curve is near point A (denoted by a solid circle) on the possible conversion plane of the ScSp arrivals at NNA. We consider that the ScSp conversion actually occurs at this point because, assuming a 10% velocity contrast between the descending slab and the surrounding mantle, the predicted ScSp/ScS amplitude ratio is about 0.1, which is consistent with the observed amplitude ratio. The local dip angle of the conversion plane (for ScSp) at this point is required to be 26°, which is also consistent with the local dip angle of the inferred upper boundary of the descending Nazca plate. Thus our revised subduction model explains both the ScSp observations and the seismicity. The ScSp observations at NNA provide strong support for the initial 30° dip of the subducting slab.

5. Concluding Remarks

Both the seismicity and the ScSp observations in central Peru are explained by our revised subduction model, which postulates that the Nazca plate descends beneath the continent with a normal dip angle (~30°) to a depth of about 100 km and then assumes an extremely shallow (near horizontal) dip angle. The focal mechanism study shows that intermediate depth earthquakes (h ≳ 70 km) within the descending slab have tension axes nearly parallel to the local dip of the slab. The orientation of tension axes suggests that at about 700-800 km inland of the trench the slab again dips at 30° and an aseismic portion of the slab may extend deeper into the mantle.

Anelasticity determinations by Sacks [1969] seem to support this suggestion. The apparent Q_s results indicate that coastal stations above the horizontal subduction area have low-frequency shear arrivals from nearby, deep earthquakes and that CUS, an inland station far from the coast, has high frequency shear arrivals. The high-Q to CUS may result from paths of low attenuation within the inland aseismic descending slab. The low-Q value at the coastal stations could be caused by the low-Q path within the mantle below the descending slab. The constraints on the model due to the anelasticity data are currently under investigation.

References

Aki, K., Earthquake generating stresses in Japan for the first motion radiation patterns, Bull. Earthquake Res. Inst. Univ. Tokyo, 44, 447-471, 1966.

Barazangi, M., and B. Isacks, Spatial distribution of earthquakes and subduction of the Nazca plate beneath South America, Geology, 4, 686-692, 1976.

Barazangi, M., and B. Isacks, Subduction of the Nazca plate beneath Peru: Evidence from spatial distribution of earthquakes, Geophys. J. R. Astron. Soc., 57, 537-555, 1979.

Isacks, B., and M. Barazangi, Geometry of Benioff zones: Lateral segmentation and downward bending of the subducted lithosphere, in Island Arcs, Deep Sea Trenches, and Back-Arc Basins, Maurice Ewing Ser., vol. 1, edited by M. Talwani and W. Pitman, pp. 99-114, AGU, Washington D.C., 1977.

Isacks, B., and P. Molnar, Distribution of stresses in the descending lithosphere from a global survey of focal-mechanism solutions of mantle earthquakes, Rev. Geophys. Space Phys., 9, 103-174, 1971.

James, D. Subduction of the Nazca plate beneath central Peru, Geology, 7, 174-178, 1978.

James, D., I. S. Sacks, E. Lazo, and P. Aparicio, On locating local earthquakes using small networks, Bull. Seismol. Soc. Am., 59, 1201-1212, 1969.

Okada, H., Converted P phases from the ScS phase at the inclined deep seismic zone, Yearb. Carnegie Inst. Washington, 72, 238-245, 1973.

Ritsema, A. R., The fault plane technique and the mechanism in the focus of the Hindu Kush earthquakes, Indian J. Meteorol. Geophys., 6, 41-50, 1955.

Sacks, I. S., Distribution of absorption of shear waves in South America and its tectonic significance, Yearb. Carnegie Inst. Washington, 67, 339-344, 1969.

Sacks, I. S., Interrelationships between volcaism, seismicity, and anelasticity in western South America, Tectonophysics, 37, 131-139, 1977.

Snoke, J. A., I. S. Sacks, and H. Okada, Determination of subducting lithosphere boundary by use of converted phases, Bull. Seismol. Soc. Am., 67, 1051-1060, 1977.

Snoke, J. A., I. S. Sacks, and D. James, Subductions beneath western South American: Evidence from converted phases, Geophys, J. R. Astron. Soc., 59, 219-225, 1979.

Stauder, W., Subduction of the Nazca plate under Peru as evidenced by focal mechanisms and by seismicity, J. Geophys. Res., 80, 1053-1064, 1975.

Sykes, L. R., Seismicity as a guide to global tectonics and earthquake prediction, Tectonophysics, 13, 393-414, 1972.